JOURNAL OF APPLIED ENGINEERING SCIENCES
ISSN: 2247-3769 / e-ISSN: 2284-7197

VOL. 15(28), ISSUE 1/2025
ART.NO. 435 pp. 29-40

ANALYSIS OF NONLINEAR BEHAVIOR AND HIGHLIGHT OF LOCAL AND GLOBAL DUCTILITY OF REINFORCED CONCRETE BEAM

M. Belhocine [a, *], K. Benyahi [a], Y. Bouafia[a], M. S. Kachi[a], A. Messas[b]

[a] Laboratory for Modeling of Materials and Structures in Civil Engineering (L2MSGC), Faculty of Construction Engineering, Mouloud Mammeri University of Tizi Ouzou, 15000 Tizi-ouzou, Algeria, E-mails: *malika.belhocine@ummto.dz, karim.benyahi@ummto.dz, youcef.bouafia@ummto.dz,mohandsaid.kachi@ummto.dz

[b] Department of Civil Engineering, Faculty of Construction Engineering, Mouloud Mammeri University of Tizi Ouzou, 15000 Tizi-ouzou, Algérie, E-mail: amar.messas@ummto.dz

Received: 10.10.2024 / Accepted: 11.12.2024 / Revised: 15.02.2025 / Available online: 31.05.2025

DOI: 10.2478/jaes-2025-0005

KEY WORDS: simulation, modeling, nonlinear behavior, local ductility, global ductility

ABSTRACT:

We are interested in modeling the nonlinear behavior of reinforced concrete framed structures. Computer tools are proposed for modeling the nonlinear behavior of deflection sections and reinforced concrete structural elements, subjected to increasing load until failure. This is done using the theory of nonlinear elasticity, which takes account of actual stress-strain curves of concrete and steel. The aim is to study the behavior in terms of local and global ductility of reinforced concrete structural elements. The analysis is carried out in the case of bent cross-sections, this enabled the moment curvature curves to be plotted and the local ductility factor to be deduced. By plotting the load displacement curves of the elements analyzed, it is possible to deduce the global ductility factor. The application of the analysis tools enabled a parametric study to be carried out into the influence of both the percentage of longitudinal reinforcement and the compressive strength of the concrete on the local and global ductility of the beam studied. The results of the validation of the « 3n beam » program are very satisfactory, confirming our results with the experimental results obtained by other authors. The parametric study shows that the global and local ductility's can vary considerably as a function of the applied stress and the percentage of longitudinal reinforcement, in particular at ω levels of 0.5 and 1%, and stresses of 25, 35 and 45 MPa, they show significant increases compared with percentages of 3 and 4% and stress 15 MPa.

1. INTRODUCTION

Under increasing loading, nonlinearities in the behavior of reinforced concrete framed structures appear. These nonlinearities can be mechanical, resulting from cracking of the concrete, plasticization of the reinforcement, and slippage between the concrete and the reinforcement. They can also be geometrical, due to the global behavior of the structure when the displacements become large. In order to obtain a realistic representation of the nonlinear behavior of reinforced concrete framed structures, nonlinear calculation methods become necessary. The contribution of computer tools has greatly facilitated the analysis of framed structural elements, designed in reinforced concrete (finite element approach), such as; LI, Q.S and Chen, J. M., 2003, Khalfallah, S and Charif., 2004; Lee, P.S and Mcclure, G., 2006; Trogrlic, B and Mihanovic, A., 2008; Belmihoub *et al.*, 2022; Ghouilem *et al.*, 2023. But no code specifies the failure loads or failure mechanisms. Current construction and design codes focus mainly on in-service and ultimate limit state performance criteria but generally do not provide explicit guidance on the loads that would cause total failure of the structure, how the structure would behave during failure (mechanism), and the actual margin between design and failure loads. Without understanding the potential failure mechanisms, it is difficult to assess the actual robustness of a structure. Knowing the actual margins would enable a more economical design while maintaining safety. This can only take place in the laboratory, where numerical calculations or structures and structural elements are pushed to extremes (to the point of failure). The main objective of nonlinear analysis of structures is to meet this expectation; this means to determine real failure loads and real failure mechanisms. The nonlinear analysis therefore consists of considering that as the load increases, plastic hinges appear each time the moment in a given section reaches the value of the plastic moment.

Reinforced concrete framed structures are the most widely used in civil and industrial construction. The finite element method has undergone considerable development in the analysis of structures. It was first used by Ngo, D and Scordolis, A.C., 1967, with a linear approach to the analysis of reinforced concrete beams. In nonlinear analysis, it was introduced by Nilson, A.H., 1968. Since then, a number of advanced studies in the field of finite element analysis of reinforced concrete structures have been published: Lin, C.S and Scordolis, A.C., 1975; Bouafia, Y.,

* Corresponding author: Malika Belhocine, Lecturer, Laboratory for Modeling of Materials and Structures in Civil Engineering (L2MSGC), Faculty of Construction Engineering, Mouloud Mammeri University of Tizi Ouzou, 15000 Tizi-ouzou, Algeria, E-mail: malika.belhocine@ummto.dz

1987; Isenberg, J., 1993; Khalfallah, S and Charif., 2004; Bouafia *et al*., 2014; Belhocine *et al*., 2023.

Several factors influence the ductility of reinforced concrete structures, such as: the compressive strength of the concrete, the percentage of tensioned and compressed reinforcement, the yield strength of the reinforcement, confinement by transverse reinforcement, and the normal force in the column. Sheikh, S.A and Uzemri, S.M., 1980; Taï, A.A., 1981; Park, R.1989; Watson *et al*, 1994; Shdeed, E and Kasoul, A, 2002, have shown that certain factors have an unfavorable effect on ductility, such as the high strength of the tensioned reinforcement and the normal stress in the elements. On the other hand, other factors have a favorable effect on ductility, namely the high compressive strength of the concrete and the high percentage of compressed reinforcement. In particular, the transverse confinement of reinforced concrete elements by rebar.

We are interested in the modeling and numerical simulation of the nonlinear bending behavior, of reinforced concrete framed elements increasing monotonic static loading, up to failure. The analysis is carried out in the case of reinforced concrete bent sections. This made it possible to plot the moment-curvature curves and deduce the local ductility factor. By plotting the load-displacement (or deflection) curves of the elements analyzed, the global ductility factor can be deduced. This modeling is carried out using the finite element method under the Navier-Bernoulli hypothesis. It is therefore discretized into finite elements of the two-node beam type« 2n beam» with six degrees of freedom (6 ddl) Belhocine *et al*, 2023. At present, we are proposing a finite element discretization of the three-node beam type «3n beam» with 9 degrees of freedom (9ddl) in order to bring more precision to the « 2n beam » program with the aim of reducing the number of iterations required to reach convergence, so the time required for the calculation is reduced.

Next, a parametric study is carried out on the influence of both the compressive strength of the concrete and the percentage of longitudinal reinforcement on the local and global ductility of a reinforced concrete beam, loaded with a fixed vertical load and an increasing lateral load until failure, using the «3n beam» and «Section» computer tools.

2. THEORICAL MODEL

2.1 Situation

We are proposing to develop two calculation tools, «3n beam » and « Section ». The first is used to simulate the global nonlinear behavior of elements such as reinforced concrete columns and beams, while the second is used to simulate the local behavior of their sections. These tools can be used to calculate resistances and displacements and to deduce the local and global ductility factors of the structures studied with respect to monotonic static loads.

2.2 Approach used

We consider the « 3n beam » element in Figure 1(a), based on the Navier - Bernoulli hypothesis operating in bending (Belhocine et al, 2023). The beam is represented by the segment gA gB in Figure 1(b):

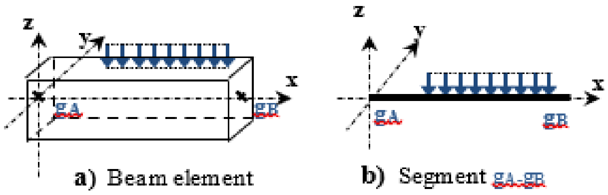

Figure 1. Bernoulli's beam element

2.3 Formulation

The relationship between deformations $\varepsilon_x(x)$ and displacements $u_0(x)$ of a point in the cross-section of the beam is linear (Eq.1):

$$\varepsilon_x(x) = \varepsilon_0(x) + z\,\phi(x) \quad (1)$$

Where

$$\varepsilon_0(x) = \frac{du_0(x)}{dx} \quad (2)$$

$$\phi(x) = -\frac{d^2w(x)}{dx^2} \quad (3)$$

$w(x, z)$: Transverse displacement along z
$u_0(x)$: axial displacement at the beam's reference axis

The relationship between forces and deformations in the cross-section is given by (Eq.4):

$$\begin{Bmatrix} N \\ M \end{Bmatrix} = \begin{bmatrix} \overline{EA} & \overline{ES} \\ \overline{ES} & \overline{EI} \end{bmatrix} \begin{Bmatrix} \varepsilon_g \\ \phi \end{Bmatrix} = [K] \begin{Bmatrix} \varepsilon_g \\ \phi \end{Bmatrix} \quad (4)$$

Where

M: Bending moment
N: Normal force
$\overline{EA}$: Normal force stiffness
$\overline{ES}$: Stiffness due to bending normal force coupling
$\overline{EI}$: Flexural rigidity
[K]: The secant stiffness matrix of the section
ε_g : Longitudinal deformation at the geometric center g of a section
ϕ : Curvature of the cross-section

In the case of non-linear behavior, the secant modulus depends on ε_g. Strain is not determined directly from stress. It is carried out by a nonlinear iterative calculation.

2.4 Finite element discretization

The discretization is performed using a finite beam element with 3 nodes and three degrees of freedom by node (or 9 degrees of freedom by element Figure 2):

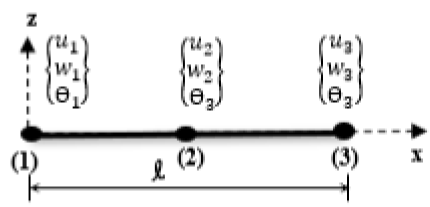

Figure 2. Three node elements

Displacements are represented by a vector of dimension 9 × 1 as follows (Eq.5):

$$u^T = \{u_1 \quad w_1 \quad \theta_1 \quad u_2 \quad w_2 \quad \theta_2 \; u_3 \quad w_3 \quad \theta_3\} \qquad (5)$$

Longitudinal displacement u_0 (x) is approximated by Lagrange-type interpolation functions of degree 2 (Eq.6):

$$u_0(x) = N_1 . u_1 + N_4 . u_2 + N_7 . u_3 \qquad (6)$$

With

u_1, u_2 et u_3 longitudinal displacement values at nodes 1, 2 and 3 respectively

Transverse displacement is approximated by Hermite interpolation functions of degree 5 (Eq.7):

$$w(x) = N_2 . w_1 + N_3 . \theta_1 + N_5 . w_2 + N_6 . \theta_2 + N_8 . w_3 + N_9 . \theta_3 \qquad (7)$$

With

w_1, w_2 and w_3: Transversal displacement values at nodes 1, 2 and 3 respectively

θ_1, θ_2, and θ_3: The values of the rotation at nodes 1, 2 and 3 respectively

$N_1, N_2, N_3, N_4, N_5, N_6, N_7, N_8$ and N_9 : Interpolation functions

The relationship between cross-sectional deformations at the element's x-axis and nodal displacements u_n is as follows (Eq.8):

$$\begin{Bmatrix} \varepsilon_{0x} \\ \phi \end{Bmatrix} = [B]\{u_n\} \qquad (8)$$

[B] : Deformation matrix

$\{u_n\}$: Nodal displacement vector

Or

$$\{u_n\} = \langle u_1 \; w_1 \; \theta_1 \; u_2 \; w_2 \; \theta_2 \; u_3 \quad w_3 \quad \theta_3 \rangle \qquad (9)$$

$$[B] = \begin{bmatrix} N_1' & 0 & 0 & N_4' & 0 & 0 & N_7' & 0 & 0 \\ 0 & -N_2'' & -N_3'' & 0 & -N_5'' & -N_6'' & 0 & -N_8'' & -N_9'' \end{bmatrix} \qquad (10)$$

$$\begin{cases} N_1(x) = -\frac{1}{2}\left(\frac{x}{l}\right)\left(1-\frac{x}{l}\right) \\ N_4(x) = \left(1-\frac{x}{l}\right)\left(1+\frac{x}{l}\right) \\ N_7(x) = \frac{1}{2}\left(\frac{x}{l}\right)\left(1+\frac{x}{l}\right) \end{cases} \qquad (11)$$

$$\begin{cases} N_2(x) = 4\left(\frac{x}{l}\right)^2 - 10\left(\frac{x}{l}\right)^3 - 8\left(\frac{x}{l}\right)^4 + 24\left(\frac{x}{l}\right)^5 \\ N_3(x) = l\left[\frac{1}{2}\left(\frac{x}{l}\right)^2 - \left(\frac{x}{l}\right)^3 - 2\left(\frac{x}{l}\right)^4 + 4\left(\frac{x}{l}\right)^5\right] \\ N_5(x) = 1 - 8\left(\frac{x}{l}\right)^2 + 16\left(\frac{x}{l}\right)^4 \\ N_6(x) = l\left[\left(\frac{x}{l}\right) - 8\left(\frac{x}{l}\right)^3 + 16\left(\frac{x}{l}\right)^5\right] \\ N_8(x) = 4\left(\frac{x}{l}\right)^2 + 10\left(\frac{x}{l}\right)^3 - 8\left(\frac{x}{l}\right)^4 - 24\left(\frac{x}{l}\right)^5 \\ N_9(x) = l\left[-\frac{1}{2}\left(\frac{x}{l}\right)^2 - \left(\frac{x}{l}\right)^3 + 2\left(\frac{x}{l}\right)^4 + 4\left(\frac{x}{l}\right)^5\right] \end{cases} \qquad (12)$$

At the level of the element's x cross-section, the relationship between internal forces and nodal displacements is evaluated using (Eq.4) and (Eq.8):

$$\begin{Bmatrix} N \\ M \end{Bmatrix} = [D][B]\{u_n\}\,;\; [D] = \begin{bmatrix} \overline{EA} & \overline{ES} \\ \overline{ES} & \overline{EI} \end{bmatrix} \qquad (13)$$

[D] : Matrix of the elastic properties of the element.

2.5 Modeling materials

Several approaches are used in the literature to describe the behavior of concrete in compression. In the present study, we use the model of Sargin, M., 1971 (Figure 3), which includes the parabolic law and the parabola-rectangle law. For the behavior of concrete in tension, we use the model of Grelat, A., 1978, which takes into account the contribution of tensioned concrete after cracking (tension stiffening effect) (Figure 4). To model the behavior of steels, we use a perfect elastoplastic law (BAEL., 1999) (Figure 5).

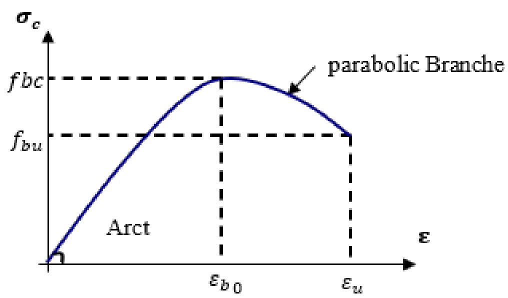

Figure 3. Behavior of concrete in compression proposed by Sargin

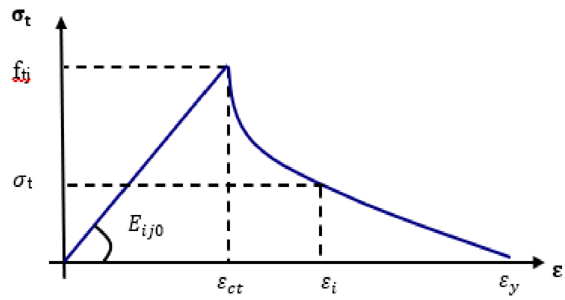

Figure 4. Behavior of concrete in tension proposed by Grelat

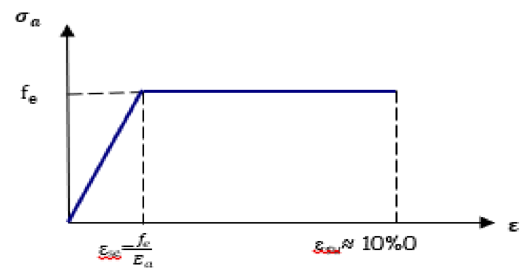

Figure 5. Law of perfect elasto-plasticity of a steel according to BAEL, 1999

Where:

f_{bc} : Compressive strength of concrete
f_{bu} : Limit compressive strength of concrete
ε_u : The maximum deformation of concrete
ε_{bo} : Peak deformation corresponding to f_{bc}
f_e: Elastic limit of steel
σ_a : Stress in the steel

ε_i : Deformation of the concrete
σ_t : Stress in concrete at the most tensioned reinforcement
ε_y : Deformation corresponding to the plasticization of steels

2.6 Flowchart for calculating the « Section and 3n beam » programs

The nonlinear resolution method in the « Section » program is carried out according to the algorithm given in Figure 1 of Appendix 1. The nonlinear analysis in the « 3n beam » program is carried out using an iterative procedure, as shown in Figure 2 of Appendix 1.

3. EXPERIMENTAL-CALCULATION CONFRONTATION AND PARAMETRIC STUDY

Firstly, we validate the « 3n beam » computer program, comparing our numerical results with the experimental results of Mazars and Low Moehle. Next, we carry out a parametric study using numerical simulations of the Mazars beam. To do this, we use the three computer tools « Section », « 2n beam» (Belhocine et *al.*, 2023) and « 3n beam » developed.

3.1 Low Moehle example

The test was carried out on a 514.4 mm high post, embedded at its base in a reinforced concrete footing. (Limkatanyu, S and Samakrattakit, A., 2003; Stanley S, Low and Jack P, Moehle., 1987), subjected to a fixed vertical load N and a variable horizontal load F variable up to failure. Two hydraulic actuators (for lateral loads) and a hydraulic jack (for axial load) were attached to the "free" end of the column through a specially fabricated universal joint. The joint allowed forces to be applied at the column end with negligible rotation. Displacements of the column were measured near the free end of the column using LVDTs (linear voltage displacement transducers). The LVDTs were mounted to a stiff reference frame attached to the footing blocks. The two versions of the program consider that the static loading is monotonic, the column is subjected to cyclic loading, so we have taken a loading cycle for. The characteristics of the materials used are presented in Table 1. The geometric characteristics of the column are shown in Figure 6.

Characteristics of concrete	
	MPa
Elasticity module E	33.10^3
Compressive strength f_{cj}	42,13
Compressive strength out concrete	44
Tensile strength f_{tj}	3.05
Poisson coefficient v	0.2

Table 1.a Characteristics of concrete

Characteristics of steel	1ereet 3eme bed	2ieme bed
	MPa	MPa
Elasticity module E	200.10^3	200.10^3
Elasticity limit	465.1	444
Resistance à la rupture	500	500
Poisson coefficient v	0.3	0.3

Table 1. b Characteristics of steel

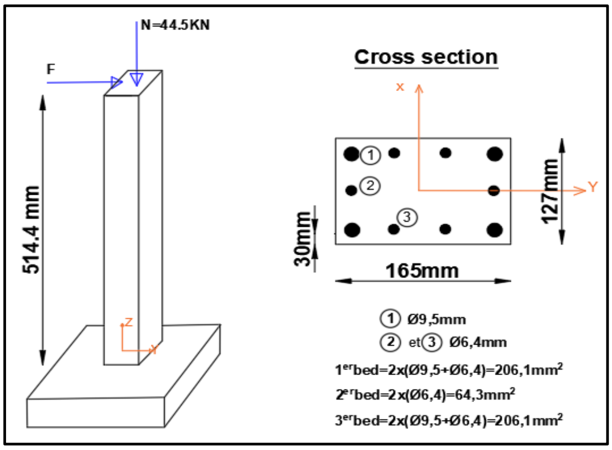

Figure 6. Geometric data of the Low Mohle column

3.2 Mazars example

The Mazars (Mazars, J., 1984) test concerns an isostatic reinforced concrete beam subjected to 3 points bending with static monotonic loading of increasing intensity, it was very important for the validation of his damage model. The test is carried out on a platform fitted with a hydraulic jack; the displacements are measured at the center of the beam with an LVDT displacement transducer. The geometric characteristics of the beam are given in Figure 7, and the main characteristics of the materials used are summarized in Table 2. The experimental curve shows the loads-deflection changes measured in the central section of the beam; flexural failure is produced by plasticization of the reinforcement (Figure 9):

Characteristics of concrete	
	MPa
Elasticity module E	$30,2 .10^3$
Compressive strength	32,3
Tensile strength f_{tj}	3.05
Poisson coefficient v	0.2

Table 2.a Characteristics of concrete

Characteristics of Steel	
	MPa
Elasticity module E	210.10^3
Elasticity limit	400
Poisson coefficient v	0.3

Table 2.b Characteristics of steel

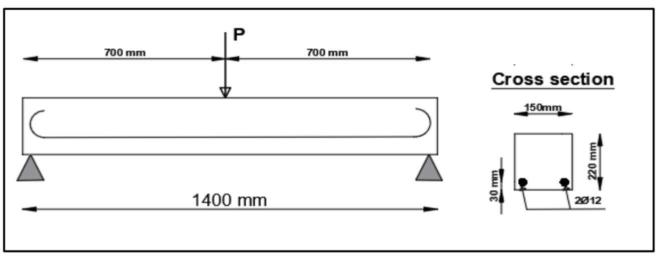

Figure 7. Geometric data for Mazars beam

4. RESULTS AND DISCUSSION

4.1 Validation of « 3n beam » program

The numerical results obtained with the «2n beam» and «3n beam» programs, compared with the experimental results of Low and Mazars, are shown in Figures 8 and 9, respectively. To see the difference between the results of the two programs, the number of elements in the discretization of the column and beam has been introduced. With a single element discretization for the low column and two elements for the Mazars beam, the «3n beam» program gives results close to the experimental results, respectively, with only 2 finite elements, satisfactory results are obtained in terms of ultimate load and maximum displacement. With the «2n Beam» program, it is from the discretization at 4 and 8 nodes that the results are close enough to the experimental results.

Compared with the «2n Beam» program, the «3n Beam» program requires fewer iterations to reach convergence, the overall calculation time can be more advantageous with the 3 node elements (2n Beam program), for the same number of elements, it gives more accurate nonlinear results, and the intermediate node allows a curvature to be represented. So, the «3n beam» program has brought more precision to the numerical results.

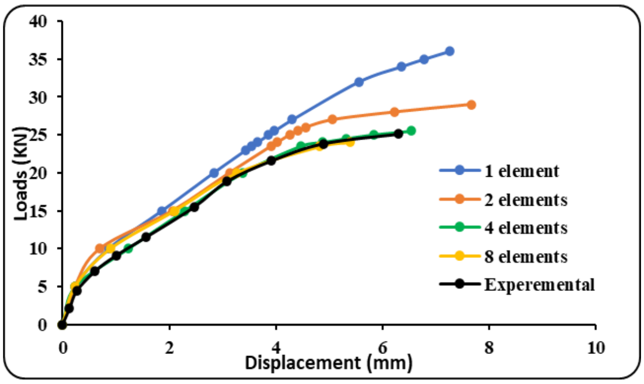

Figure 8. a Experimental and calculated load-deflection curves for Low column with «2n beam» program

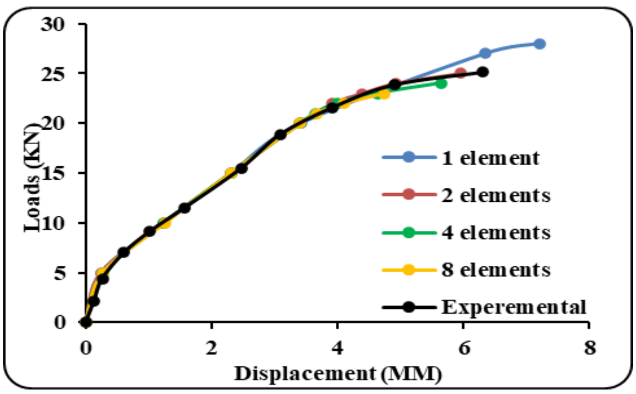

Figure 8. b Experimental and calculated load-deflection curves for Low Moehle column with «3n beam» program

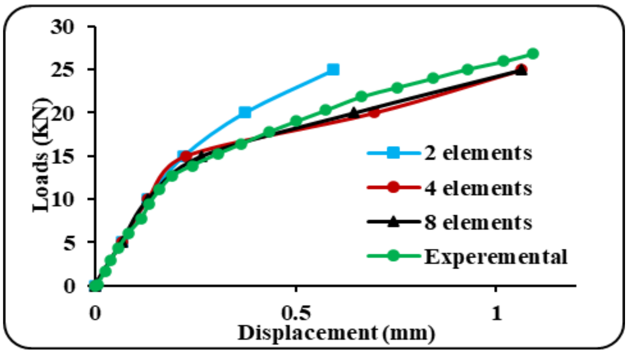

Figure 9. a Experimental and calculated load-deflection curves for the Mazars beam column with «2n beam» program

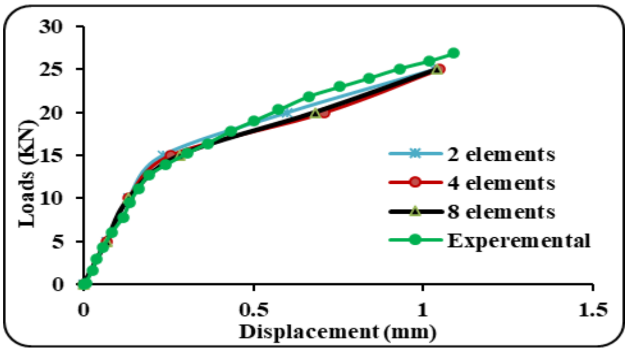

Figure 9. b Experimental and calculated load-deflection curves for the Mazars beam with «3n beam» program

4.2 Parametric study results

To see the influence of the percentage of longitudinal reinforcement ω (ω = As/B (%)) and the compressive strength f_{cj} on the nonlinear behavior of the Mazars beam keeping the same geometric cross-section, we carried out several numerical simulations, considering several values of ω and f_{cj}. According to the rules of the Algerian earthquake regulations (RPA, 2003), the minimum reinforcement of a rectangular section (B) of the beams is 0.5% of B, and the maximum reinforcement is 4% of B. The values of the compressive strength f_{cj} are between 15 MPa and 50 MPa; these values correspond to those that can be encountered in practice for ordinary concrete.

Ductility is a very important criterion that describes the behavior of structures and their degree of energy dissipation in the plastic domain. In this study, the global ductility of the beam using the curve load-displacement given by the program «3n beam» is calculated by the factor $\mu_D = D_u/D_y$, which represents the maximum displacement achieved D_u over the elastic displacement D_y of the beam. The local ductility of the beam using the curve load-curvature given by the program «Section» is calculated by the factor: $\mu_\phi = \phi_u/\phi_y$, which represents the maximum curvature achieved ϕ_u over the elastic curvature ϕ_y of the beam.

4.2.1 Influence of compressive strength and longitudinal reinforcement at beam level (global ductility)

The numerical results obtained after calculations with the program «3n beam», varying both the compressive strength f_{cj} and the percentage of longitudinal reinforcement ω at the Mazars beam (keeping the same geometric cross-section of the beam), are presented in Table 1 (appendix 2) and Figures 10-20. They show that the ultimate load capacity increases with increasing percentage ω from an average of 49% to 10% and increases by 5% by raising the strength f_{cj}; the maximum displacement also increases with ω. For ω = 0.5, all the stresses reach their maximum global ductility, with particularly high ductility for the 25 Mpa stress (μ_D = 6.01). Beyond this value, ductility decreases, with a difference of 37% to 3% for excess reinforcement. Global ductility increases with a 7% increase in resistance f_{cj}. The work of Sheikh, S.A and Uzemri, S.M., 1980; Park, R.1989; Belhocine *et al.*, 2023, shows that global ductility decreases with an excess of longitudinal reinforcement (ω).

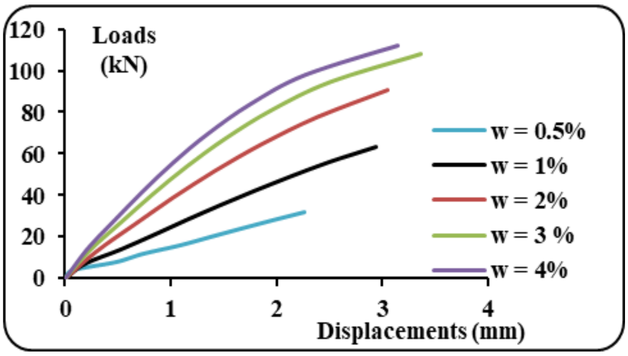

Figure 10. Load displacement curves for the beam, for f_{cj} = 15 Mpa as a function of ω

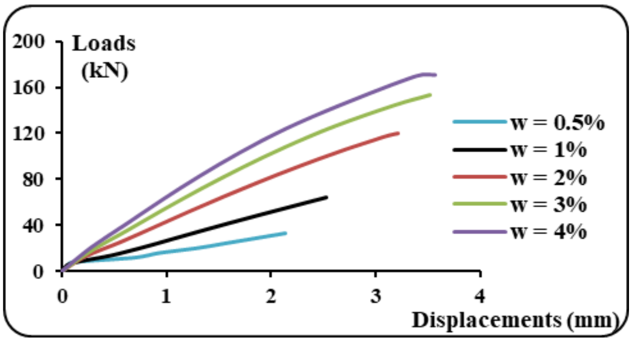

Figure 11. Load displacement curves of the beam for f_{cj} = 25 Mpa as a function of ω

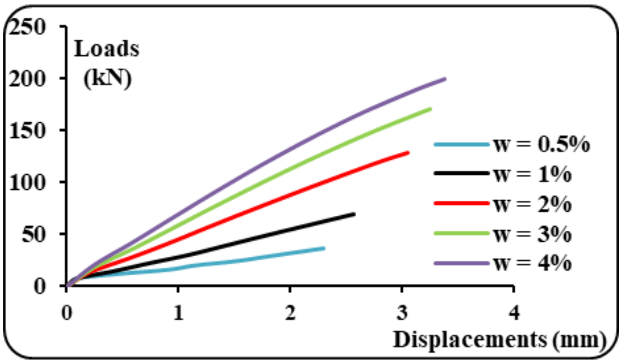

Figure 12. Load displacement curves for the beam, for f_{cj} = 35 Mpa as a function of ω

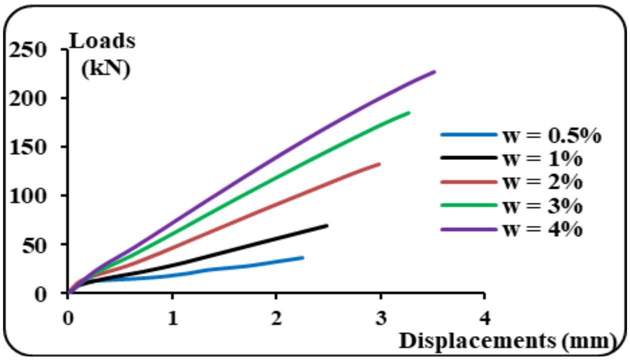

Figure 13. Load displacement curves of the beam, for f_{cj} = 45 Mpa as a function of ω

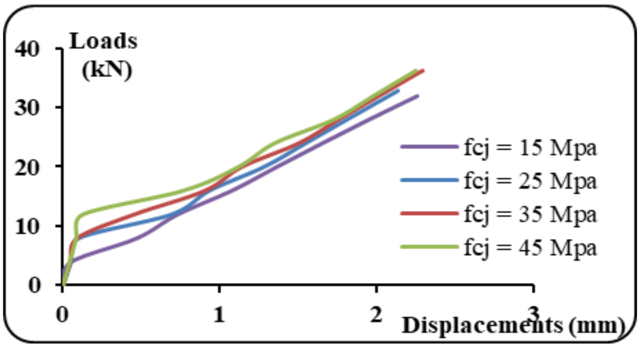

Figure 14. Load displacement curves for the beam, for ω = 0.5 % as a function of f_{cj}

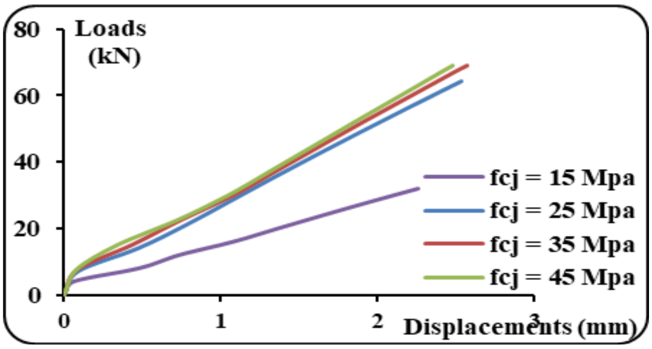

Figure 15. Load displacement curves for the beam for ω = 1% as a function of f_{cj}

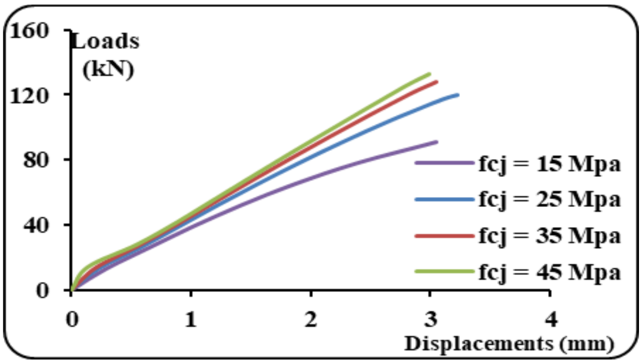

Figure 16. Load displacement curves for the beam, for ω = 2 % as a function of f_{cj}

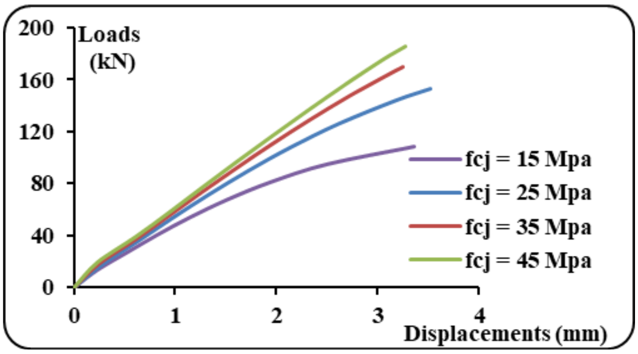

Figure 17. Load displacement curves for the beam, for ω = 3% as a function of f_{cj}

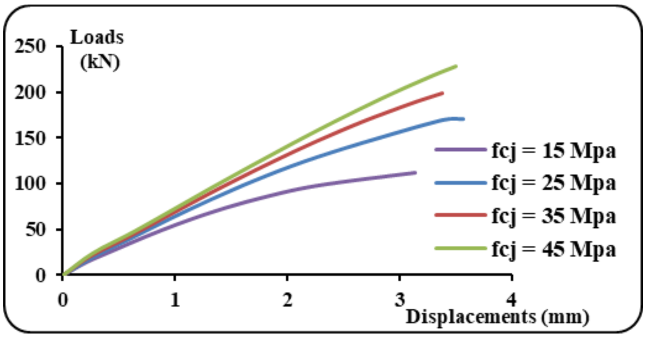

Figure 18. Load displacement curves for the beam, for ω = 4% as a function of f_{cj}

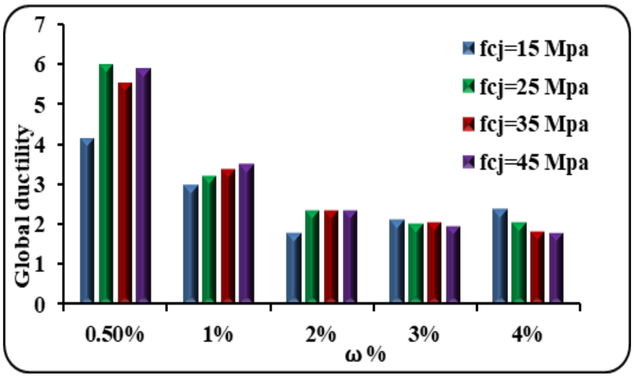

Figure 19. Variation in global ductility by varying stress f_{cj} as a function of percentage of reinforcement ω

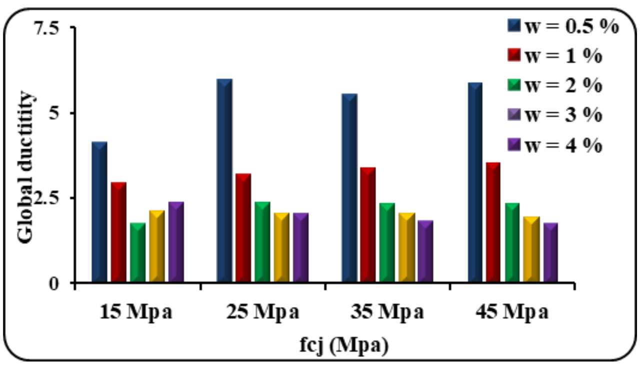

Figure 20. Variation in global ductility by varying the percentage of reinforcement ω as a function of stress f_{cj}

4.2.2 Influence of compressive strength and longitudinal reinforcement on the beam section (local ductility)

The numerical results obtained with the « Section » program, by varying both the compressive strength f_{cj} and the percentage of longitudinal reinforcement ω, at the section level of the Mazars beam (keeping the same geometric cross-section of the beam), are presented Table 2 (appendix 2) and Figures 21-31. They show that the moment M_{max} of failure increases with the percentage of reinforcement from an average of 46% to 2%.

It can be seen that the local ductility increases by 33% as a function of the percentage of longitudinal reinforcement ω up to the value 1%, then decreases from 34% to 0% for a heavily reinforced section. For ω = 1%, all stresses reach their maximum ductility, with particularly high ductility for the stress of 45 Mpa (μ_D = 3.73). The section has shown sufficiently ductile behavior; beyond this value, the behavior becomes brittle (μ_D = 1 for 3% and 4%).

Local ductility increases with increasing stress up to 2%; beyond this, it is particularly stable at 3% and 4% of ω, where the ductility values for compressive stress 35 Mpa and 45 MPa are significantly lower than for the other compressive stresses (μ_ϕ = 1). Sheikh, S.A and Uzemri, S.M., 1980; Park, R.1989; M. Belhocine *et al.*, 2023, have shown that an excess of tensioned reinforcement degrades the local ductility of the beam section.

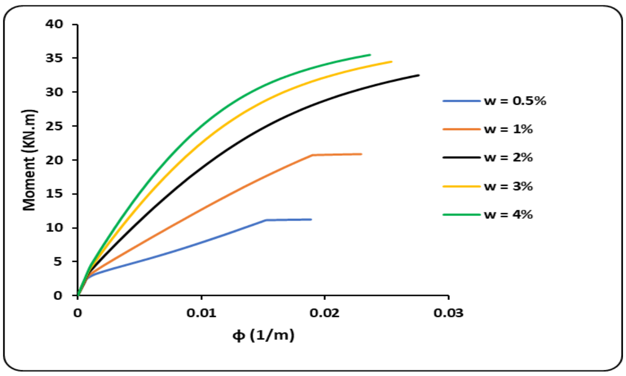

Figure 21. Moment curvature curves of the beam, for f_{cj} = 15 Mpa as a function of ω

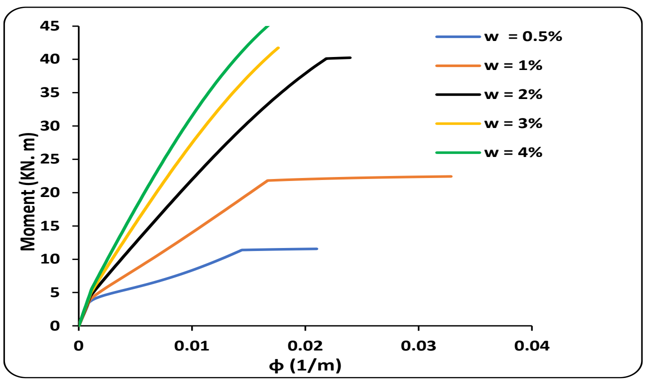

Figure 22. Moment curvature curves of the beam, for f_{cj} = 25 Mpa as a function of ω

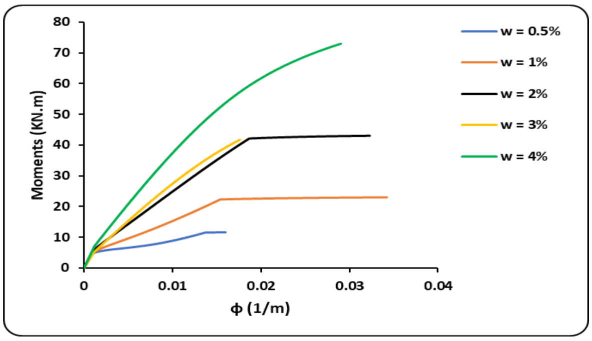

Figure 23. Moment curvature curves of the beam, for f_{cj} = 35 Mpa as a function of ω

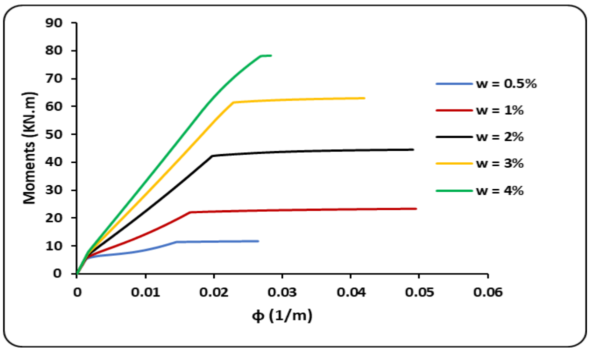

Figure 24. Moment curvature curves of the beam, for f_{cj} = 45 Mpa as a function of ω

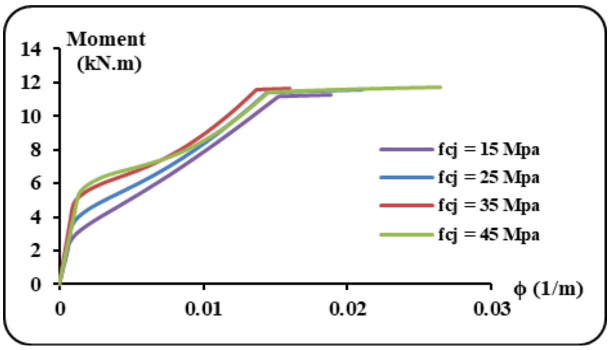

Figure 25. Moment curvature curves of the beam, for ω = 0.5% as a function of f_{cj}

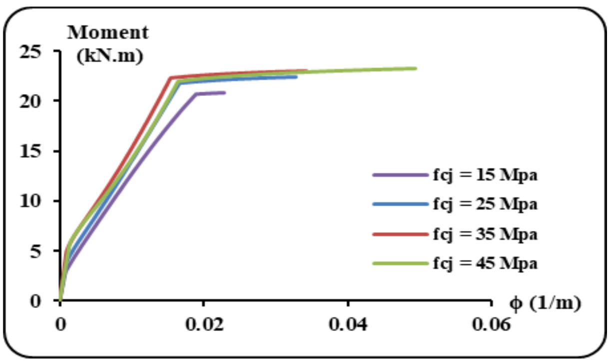

Figure 26. Moment curvature curves of the beam, for ω = 1% as a function of f_{cj}

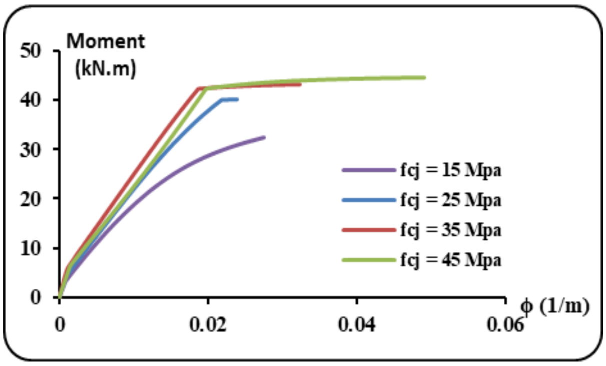

Figure 27. Moment curvature curves of the beam, for ω = 2% as a function of f_{cj}

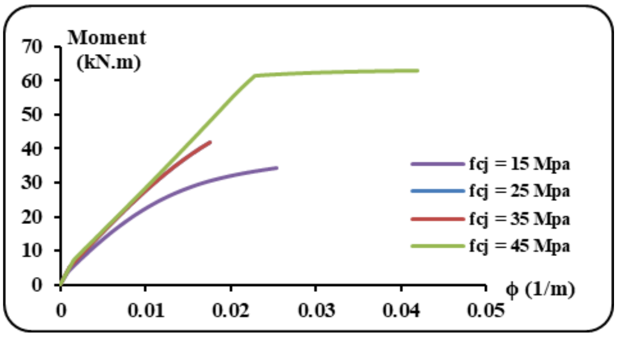

Figure 28. Moment curvature curves of the beam, for ω = 3% as a function of f_{cj}

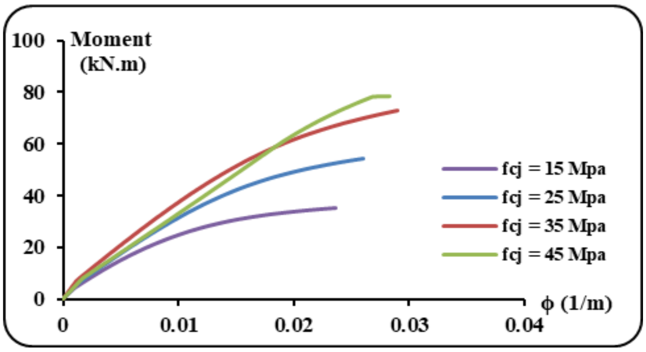

Figure 29. Moment curvature curves of the beam, for ω = 4% as a function of f_{cj}

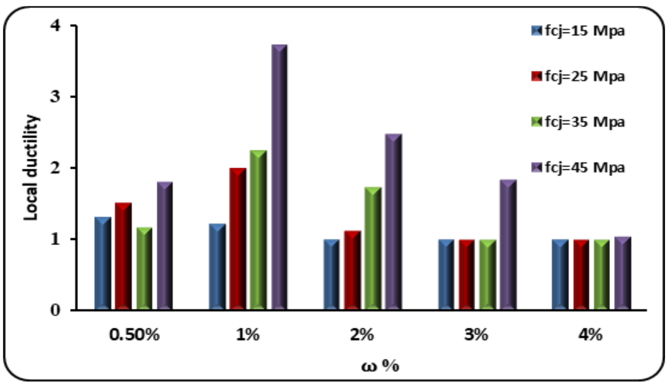

Figure 30. Variation in local ductility by varying stress f_{cj} as a function of percentage ω

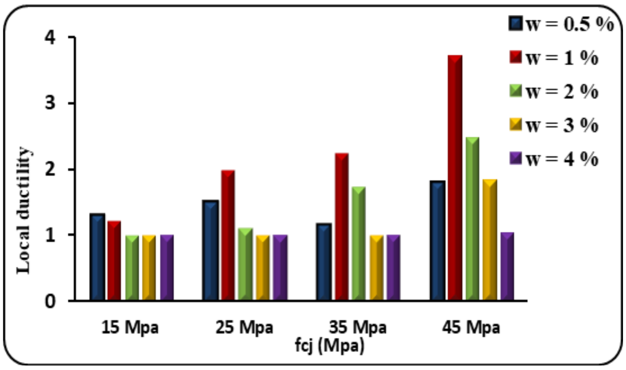

Figure 31. Variation in local ductility by varying the percentage ω as a function of f_{cj}

5. CONCLUSION

The results of the validation of « 3n beam » program are satisfactory by comparing the results with those obtained with « 2n beam » the experimental results calculated by Mazars and Low. the « 3n beam » program has brought more precision to the numerical results. The «3n Beam» program requires fewer iterations to reach convergence, so the overall calculation time can be shorter than that given by the «2n beam» program.

A parametric study was carried out on the influence of various parameters on the local and global ductility of Mazars beam, namely the compressive strength of the concrete and the percentage of longitudinal reinforcement. It was found that both local and global behavior appeared to be affected by these parameters. From this parametric study, we have drawn the following remarks:

- The moment M_{max} at failure increases with the increase in the percentage of reinforcement with an average of 46% at 2%, the curvatures increase then decrease with the increase in f_{cj} and ω.
- The breaking load capacity increases with increasing percentage ω from an average of 49% to 10%, the maximum displacement also increases with ω.
- The local ductility increases by 33% as a function of the percentage of longitudinal reinforcement ω up to the value of 1%, then decreases from 34% to 0% for a heavily reinforced section. For ω = 1%, all stresses reach their maximum ductility, with particularly high ductility for the stress of 45 MPa (μ_D = 3.73, the section has shown sufficiently ductile behavior), beyond this value the behavior becomes brittle (μ_D = 1 for 3% and 4%).
- Local ductility increases with increasing stress up to 2%, beyond which it is particularly stable at 3% and 4% of ω, where the ductility values for 35 and 45 MPa are significantly lower than those for the other stresses.
- For ω = 0.5, all stresses reach their maximum overall ductility, with particularly high ductility for the 25 MPa stress (μ_D = 6.01). Beyond this value, ductility decreases, with a difference of 37% to 3%, for excess reinforcement.
- Local and global ductility increase by around 29% and 5% respectively as a function of the concrete compressive strength f_{cj}, and the strength capacity also increases as a function of f_{cj}.

These results show that the global and local ductility can vary considerably with the applied stress and the percentage of reinforcement, in particular at ω levels of 0.5% and 1%, and stresses of 25, 35 and 45 MPa, they show significant increases compared with percentages of 3 and 4% and stress 15 MPa respectively. The local ductility still remains lower than the overall ductility of the beam.

In terms of perspectives, we can envisage taking into account:

- Displacements due to shear forces,
- The behavior of three-dimensional structures with the effect of torsion in the global modelling of this type of structure.

References

A. Asghar, Taï., 1981. Analyse de la tenue aux séismes des structures en béton armé. Prise en compte globale des non-linéarités, Doctoral Thésis, Ecole Nationale des Ponts et Chaussées, France.

Y, Bouafia., 1987. Simulation numérique du comportement moyen, jusqu'à rupture, d'une zone de poutre. Application au béton armé ou précontraint et béton de fibres. Mémoire DEA, Université de Paris 6, 77 p.

Grelat, Alan., 1978. Comportement non linéaire et stabilité des ossatures en béton armé. *Annales de l'institut technique de bâtiment et de travaux publics*, série: théories et méthodes de calculs 223, n°366, p 105-126.

H, Belmihoub., A, Hamza and N, Mesboua., 2022. Modelling of in earthen dam under the effect of seismic loading-case of the taksebt dam (Algéria). *Journal of applied engineering sciences*, Vol. 12(25) issue 1, page 17-26. DOl: 10.2478/jaes-2022-0003

K, Ghouilem., D, Atlaoui and S, Merakeb., 2023. Creep behavior of the clay cores at the Bougdora dam using ANSIS software. *Journal of applied engineering sciences*, Vol. 13(26) issu 2, Art. No. 374, pp. 189-196. DOI: 10.2478/jaes-2023-0024

Lee, P.S and Mcclure, G., 2006. A general three-dimensional L-section beam finite element for elastoplastic large deformation analysis. *Computers and Structures 84*, pages 215-229.

Limkatanyu, S and Samakrattakit, A., 2003. Frame element including effects of reinforcement slippage for nonlinear analysis of R/C structures. *Songklanakarin Journal of Science and Technology*, Vol. 25 No. 2, pp. 213-226.

LI, Q.S and Chen, J. M., 2003. Non-linear elastoplastic dynamic analysis of single layer reticulated shells subjected to earthquake excitation. *Computers and Structures 81*, pages 177-188.

Malika, Belhocine., Youcef, Bouafia., Mohand Said, Kachi and karim, Benyahi., 2023. Assessment of nonlinear behavior and ductility of reinforced concrete structures. *World Journal of Engineering*, Vol. 20 No. 3, pp. 522-543. https://doi.org/10.1108/WJE-03-2021-0181

Mazars, J., 1984. Application de la mécanique de l'endommagement au comportement nonlinéaire et à la rupture du de structure. Thèse doctorat d'état, université Pierre Marie Curie paris 6.

Ngo, D and Scordelis, A.C., 1967. Finite element analysis of reinforced concrete. *A.C.I journal*, N°64-14, pp.152- 163.

Nilson, A.H., 1968. Non-linear analysis of reinforced concrete by finite element method. *A.C.I journal*, N°65-55, pp.757- 766.

Park, R., 1989. Evaluation of ductility structures and structural assemblages from laboratory testing. *Bulletin of the New Zeland National Society for Earthquake Engineering*, Vol.22 No. 3, pp. 155-165. https://doi.org/10.5459/bnzsee.22.3.155-166

RPA. Règlement Parasismique Algerian 2003. Algerian seismic code, *National Center for Applied Research in Earthquake Engineering*, RPA99, Algiers, Algeria.

Rules BAEL 91, revised 99. 1999. Technical rules for the design of reinforced concrete structures according to the limit states method, Publisher: Association Française de Normalization.

Sargin, M., 1971. Stress – strain relationships for concrete and the analysis of the structural concrete sections. *Solid Mechanics Division*, University of Waterloo, S M study n° 4 Canada.167p.

Shdeed, E and Kasoul, A., 2002. Prise en compte de la ductilité dans les Méthode de renforcement des anciens bâtis. *Journal of the structural division*, Vol 108, pp. 1079-1102.

Sheikh, S.A. and Uzemri, S.M., 1980. Strength and ductility of tied in reinforced concrete columns". *Journal of the structural division*, Vol. 108, pp .1079-1102.

S, Khalfallah, and A, Charif., 2004. Modélisation du comportement non linéaire des structures en béton armé. *Sciences et technologie*, B – N°21, pp. 29-35.

Trogrlic, B and Mihanovic, A.**,** 2008, The comparative body model in material and geometric nonlinear analysis of space R/C frames. *Engineering Computations*, Vol. 25 No. 2, pp. 155-171. https://doi.org/10.1108/02644400810855968

Stanley S, Low and Jack P, Moehle., (1987), Experimental study of reinforced concrete column subjected to multy-axial cyclic loading. *Earthquake Engineering Research Center*. Report NO UCB/EERC. 87/14.

Watson, S., Zahn, F and Park, R., 1994. Confining reinforcement for concrete columns, *Journal of Structural Engineering*. 120(6), 1798–1824. Https ://doi. org/10.1061/(ASCE)0733-9445(1994)120:6(1798).

Y, Bouafia., A, Iddir., M.S, Kachi and H, Dumontet., 2014. Stress–strain relationship for the confined concrete. *Stress MPa*, vol. 70, p. 80.

Isenberg, J., 1993. Finite element analysis of reinforced concrete structures II. *ASCE*, ed. New York.

Appendix 1:

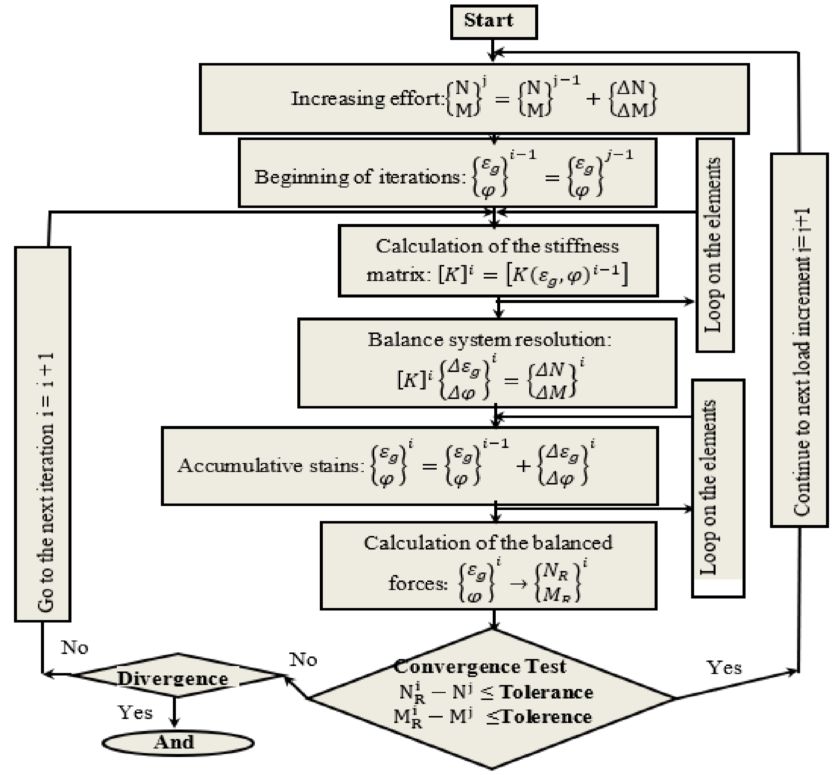

Figure 1. Calculation flowchart at section level (Section program)

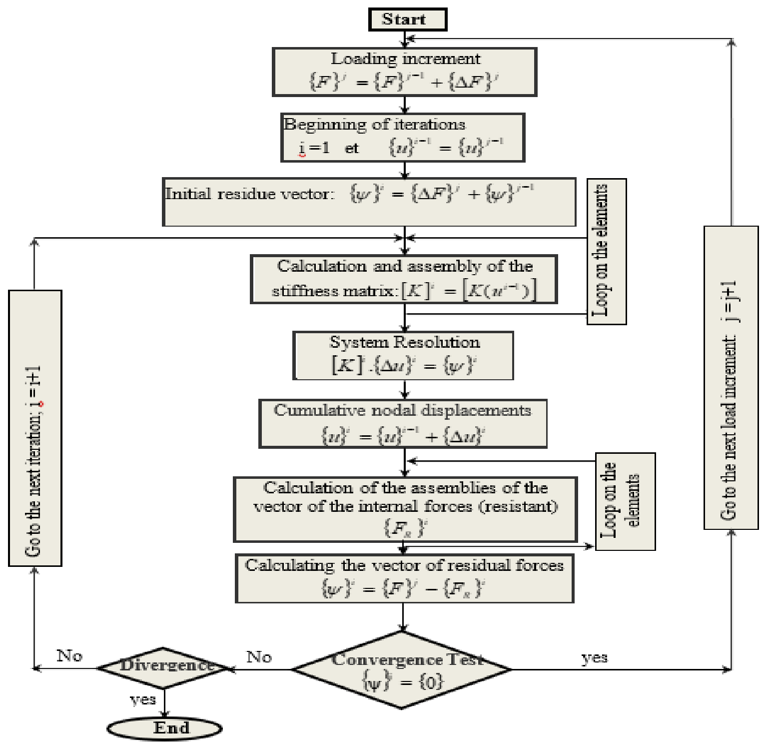

Figure 2. Structural design flowchart (3n beam program)

Appendix 2:

f_{cj}	ω	D_u	D_y	$\mu_D = D_u/D_y$
(Mpa)	(%)	(mm)	(mm)	
15	0.5	2.2617	0.54132	**4.17**
	1	2.9404	0.98512	**2.98**
	2	3.0483	1.697	**1.79**
	3	3.3635	1.5787	**2.13**
	4	3.1428	1.3059	**2.4**
25	0.5	2.1423	0.35616	**6.01**
	1	2.5347	0.78396	**3.23**
	2	3.2208	1.3497	**2.38**
	3	3.5176	1.7165	**2.04**
	4	3.5704	1.7152	**2.08**
35	0.5	2.2998	0.41366	**5.56**
	1	2.5698	0.75759	**3.39**
	2	3.0943	1.3132	**2.35**
	3	3.4026	1.6428	**2.07**
	4	3.379	1.8304	**1.84**
45	0.5	2.2531	0.38171	**5.9**
	1%	2.4822	0.70103	**3.54**
	2%	2.9835	1.2655	**2.35**
	3%	3.2736	1.6666	**1.96**
	4%	3.5071	1.9538	**1.79**

Table 1. Numerical results given by “3n beam” program

f_{cj}	ω	ϕ_u	ϕ_y	$\mu_\phi = \phi_u/\phi_y$
(Mpa)	(%)	(1/m)	(mm)	
15	0.5	0.01886	0.01424	**1.32**
	1	0.02292	0.01870	**1.22**
	2	0.02757	0.02757	**1**
	3	0.02537	0.02537	**1**
	4	0.02363	0.02363	**1**
25	0.5	0.02099	0.01388	**1.51**
	1	0.03285	0.01641	**2**
	2	0.02427	0.02175	**1.12**
	3	0.01760	0.01760	**1**
	4	0.02605	0.02605	**1**
35	0.5	0.01599	0.01361	**1.17**
	1	0.03421	0.01515	**2.25**
	2	0.03228	0.01858	**1.73**
	3	0.0176	0.0176	**1**
	4	0.02902	0.02902	**1**
45	0.5	0.02643	0.01397	**1.81**
	1	0.06152	0.01647	**3.73**
	2	0.04905	0.01963	**2.49**
	3	0.04194	0.02263	**1.85**
	4	0.02830	0.02678	**1.05**

Table 2. Numerical results given by “Section” program